

Room-temperature Coulomb blockade from a self-assembled molecular nanostructure

M. Dorogi

Department of Physics, Purdue University, West Lafayette, Indiana 47907

J. Gomez

Departamento de Física de la Materia Condensada, Universidad Autonoma de Madrid, Madrid, Spain

R. Osifchin and R.P. Andres

School of Chemical Engineering, Purdue University, West Lafayette, Indiana 47907

R. Reifengerger

Department of Physics, Purdue University, West Lafayette, Indiana 47907

(Received 27 October 1994; revised manuscript received 12 April 1995)

Nanometer-size Au clusters deposited from a cluster beam onto a thin dithiol film were studied at room temperature using an ultrahigh vacuum scanning tunneling microscope (STM). The dithiol molecules tether the deposited Au clusters to the underlying gold substrate and repeatable STM scans of the Au clusters were achieved. Data of the tunneling current as a function of applied voltage yield reproducible evidence for single-electron tunneling at room temperature. By fitting the measured $I(V)$ data to a Coulomb blockade model, estimates for the electrical resistance of a single dithiol molecule are also obtained.

I. INTRODUCTION

The ability to form high-quality monolayer films of alkanethiols using a self-assembly process makes the study of thiol-based organic films an interesting topic.¹⁻³ The use of self-assembled monolayers (SAM's) to support metallic particles formed from the aggregation of evaporated metal atoms has suggested that weak electronic coupling between the aggregates and the underlying gold substrate can be achieved.⁴ However, other studies utilizing ion-scattering spectroscopy contradict the notion that metal atoms evaporated onto alkanethiol SAM's at room temperature form supported structures isolated from the substrate. The ion-scattering data show that at room temperature, evaporated metal atoms penetrate the organic monolayer and form adclusters on the surface of the underlying substrate.⁵ This finding is consistent with the dynamic nature of alkanethiol SAM's at room temperature, where defects can be annealed out using a modest temperature increase.⁶

In what follows, we report results of a study which extends this previous work in two important ways. First, instead of relying on atoms vacuum evaporated onto organic monolayers to form small metal aggregates isolated from a substrate, we use nanometer-size Au clusters, preformed and annealed in an inert gas stream. This process produces single-crystal particles having a fcc structure.⁷ Au clusters produced in this manner were vacuum deposited on SAM covered Au substrates. Second, instead of using single-ended alkanethiol molecules, we employ a double-ended thiol molecule, *p*-xylene- α , α' -dithiol ($C_8H_{10}S_2$), hereafter referred to as XYL dithiol, to form SAM's on atomically flat Au(111) films. The XYL dithiol

SAM links the Au cluster to the organic film via covalent Au-S bonds. The well defined nanostructure under study is shown schematically in Fig. 1.

Following this approach, reliable images of single supported clusters could be obtained at room temperature using a scanning tunneling microscope (STM). This is an important result since prior attempts to image preformed clusters on atomically flat substrates using scanning probe microscopy have proven difficult due to strong tip-cluster interactions.⁸ Only recently has it been possi-

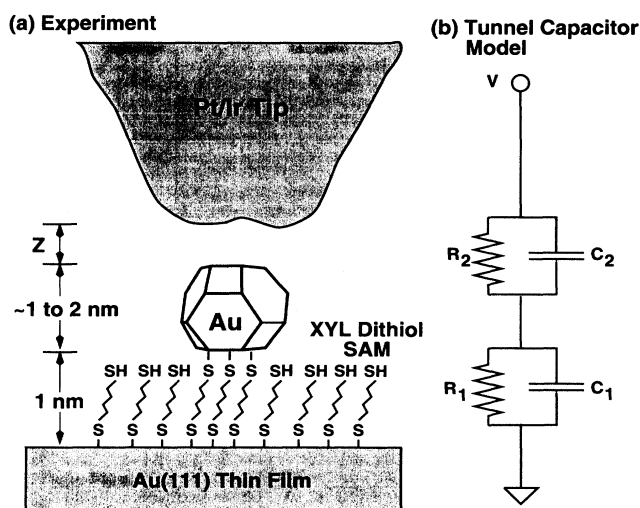


FIG. 1. (a) Schematic diagram of the nanostructure studied. (b) Double junction model used to explain the $I(V)$ data.

ble to image preformed clusters supported on atomically flat substrates using noncontact atomic force microscopy (AFM).⁹ Reliable imaging of the clusters with scanning tunneling microscopy allows the current-voltage characteristics of an individual supported cluster to be studied. $I(V, z)$ data taken at room temperature under UHV conditions provide evidence for single-electron tunneling effects, indicating a weak electronic coupling of the clusters to the underlying substrate. Analysis of this data also allows an estimate of the electrical resistance of a single XYL dithiol molecule.

II. EXPERIMENTAL TECHNIQUES

A. Cluster source

The clusters studied here were prepared using a multiple expansion cluster source (MECS) as described elsewhere.^{10–12} The MECS is a gas aggregation source, designed to run with 20–50 torr of inert gas in the growth region. Both cluster growth via accretion of single atoms and via cluster-cluster aggregation can be promoted. In the present experiments, Au clusters with diameters of ~ 2 nm were produced. As in previous studies,^{13–18} cluster samples were captured either on sample substrates for scanning probe analysis or on 5 nm thick amorphous carbon films supported on 400 mesh grids for analysis by TEM. Before deposition onto a substrate, the Au clusters are melted and recrystallized in the gas phase. Previous high-resolution TEM studies of Au clusters show that after such gas phase annealing, the clusters are single fcc crystals.⁷ Total energy calculations indicate that for the Au clusters used in this study, a truncated octahedral structure is the preferred cluster shape. As will be discussed later, knowledge of the cluster structure can be used to calculate the contact area between the cluster and the organic XYL dithiol layer, allowing a good estimate of the number of XYL dithiol molecules supporting an individual Au cluster.

B. UHV STM system

The STM used for these studies is a homebuilt system which uses a computer controlled digital feedback system for imaging¹⁹ and spectroscopy.²⁰ The STM is housed in a multichamber UHV system which includes a sample/tip insertion chamber, a sample preparation chamber, and the STM chamber. The STM chamber operates at a base pressure of 3×10^{-10} torr. The entire system is supported by three vibration-isolation legs which are mounted on an optical table. The STM was calibrated in the XY direction by imaging a 200 nm grating and atoms on highly oriented pyrolytic graphite (HOPG). In the Z direction it was calibrated with monoatomic steps on Au(111). The STM tips were etched PtIr wires (0.25 mm diameter), cleaned by field emission in the STM chamber.

$I(V, z)$ measurements were made using a signal averaging technique. A predetermined number of $I(V)$ sweeps (typically 100) are taken with the tip position determined

by an initial preset tunnel current and bias voltage. The tip position is adjusted prior to each individual $I(V)$ sweep, so the effect of piezodrift is minimized. After completing data acquisition for one current set point, the data was averaged, and the set point was incremented to allow data acquisition for another tip separation. This procedure is repeated for six different tunnel current set points.

$I(V, z)$ spectroscopic measurements were taken simultaneously with topographic data in the following way. A feature of interest was first centered in the STM image using the normal imaging mode. Then, while acquiring an image, the tip was paused in the center of the image and an $I(V, z)$ measurement was made. After acquiring the $I(V, z)$ data, the STM image was finished. This method has the advantage that the exact position of the $I(V, z)$ measurement is known. Any tip switches or effects due to thermal drift can easily be seen in the STM image.

C. Sample preparation

Au(111) films typically 150 nm thick were prepared by thermal evaporation of high-purity Au onto mica substrates heated to 350 °C. Scans of the Au(111) films showed that they were atomically flat over dimensions of a few square μm with step edges clearly visible.²¹ SAM's were prepared by soaking the Au films in a dilute solution of XYL dithiol in methylene chloride for 12 to 24 h, followed by rinsing with ethanol and drying with nitrogen gas.

The Au/XYL dithiol films prepared in this way have been characterized by ellipsometry, Raman, contact angle, and IR spectroscopy and found to be ordered SAM's.²² From ellipsometry, the thickness of the XYL dithiol layer was found to be 0.83 nm with a dielectric constant of ~ 1.5 . The expected layer thickness is 0.77 nm.

The Au(111)/XYL dithiol films were inserted into a vacuum chamber held at $\sim 10^{-6}$ torr for cluster deposition. They were exposed to a molecular beam of ~ 2 nm diameter, annealed Au clusters. The TEM samples were exposed to the same cluster flux as the Au(111)/XYL dithiol films. After cluster deposition, the Au(111)/XYL dithiol/cluster samples were inserted into the UHV STM for further study at room temperature. The TEM samples were used to provide independent information about the cluster coverage and the size distribution of the deposited clusters.

III. RESULTS

A. Cluster size

From their STM images, the apparent diameters of the Au clusters were found to range between 5 and 10 nm. A TEM micrograph of the same clusters deposited on a thin carbon film gave an average diameter of 1.9 ± 0.6 nm. It can be concluded that the STM images are considerably broadened by tip convolution effects.

If the Au clusters do not strongly interact with the XYL dithiol film, the average cluster diameter obtained from the TEM micrograph should equal either the average cluster height obtained from the STM study or this height minus a small offset to account for the height of the dithiol film. To check this, a height distribution of the clusters was obtained from many STM images, yielding an average height of 1.4 ± 0.6 nm. From this result, it appears that the clusters are slightly flattened. A similar result using noncontact AFM to image Au clusters supported on various flat substrates has been reported elsewhere.²³

It is not clear why the clusters appear flattened when imaged with the STM. The observed flattening may be indicative of an interaction between the clusters and the underlying film which deforms the clusters. It is also possible that the clusters burrow into the organic film or that the organic film is compressed as the STM tip scans across the cluster. More work is required before the origin of this effect can be clearly elucidated.

B. $I(V, z)$ data on a tethered cluster nanostructure

Because of the long-term stability of these samples, it was possible to obtain reliable $I(V, z)$ spectra as described in Sec. II B. It is interesting to compare data taken when the tip is over a cluster and when it is over the XYL dithiol layer. Typical data are shown as a function of the tunnel current set point (i.e., tip-cluster separation) in Figs. 2 and 3, where two distinct shapes of the $I(V, z)$ data are evident. When the tip is centered over a cluster, suppression of the tunnel current at zero bias voltage is found, suggesting the presence of a room-temperature Coulomb blockade. When the tip is over the XYL dithiol film, a reasonably linear $I(V)$ curve results.

In order to characterize the electronic properties of the molecular nanostructure, a fit to this data was performed using published theories^{24–26} for a double-junction tunnel capacitor. In this model, two tunnel capacitors shown schematically in Fig. 1(b) are biased by applying a voltage V_{bias} across the array. Each junction has a capacitance, an effective resistance, and a tunneling rate associated with it, denoted by C_i, R_i , and Γ_i , with $i = 1, 2$. In principle, a fractional charge Q may exist on a cluster, permitting the entire $I(V)$ data to be shifted to the left or right of the origin. Q also adds some asymmetry to the detailed shape of the $I(V)$ curve. In analyzing the experimental results presented here, the parameter Q was not required due to the symmetric nature of the data obtained.

Based on the tunnel capacitor model, a computer program was developed which calculates a best fit to $I(V)$ data for a two-junction array by searching over a wide range of parameter space. A best fit amounts to finding a global minima in the mean-square deviation of a theoretical $I(V)$ calculation from experimental data while allowing the capacitances and resistances, and possibly T to vary. Since neither $I(T, V; C_1, C_2, R_1, R_2)$ nor its partial derivatives can be represented analytically, finding a global best fit is computationally intensive. A traditional technique such as the “method of steepest descent”

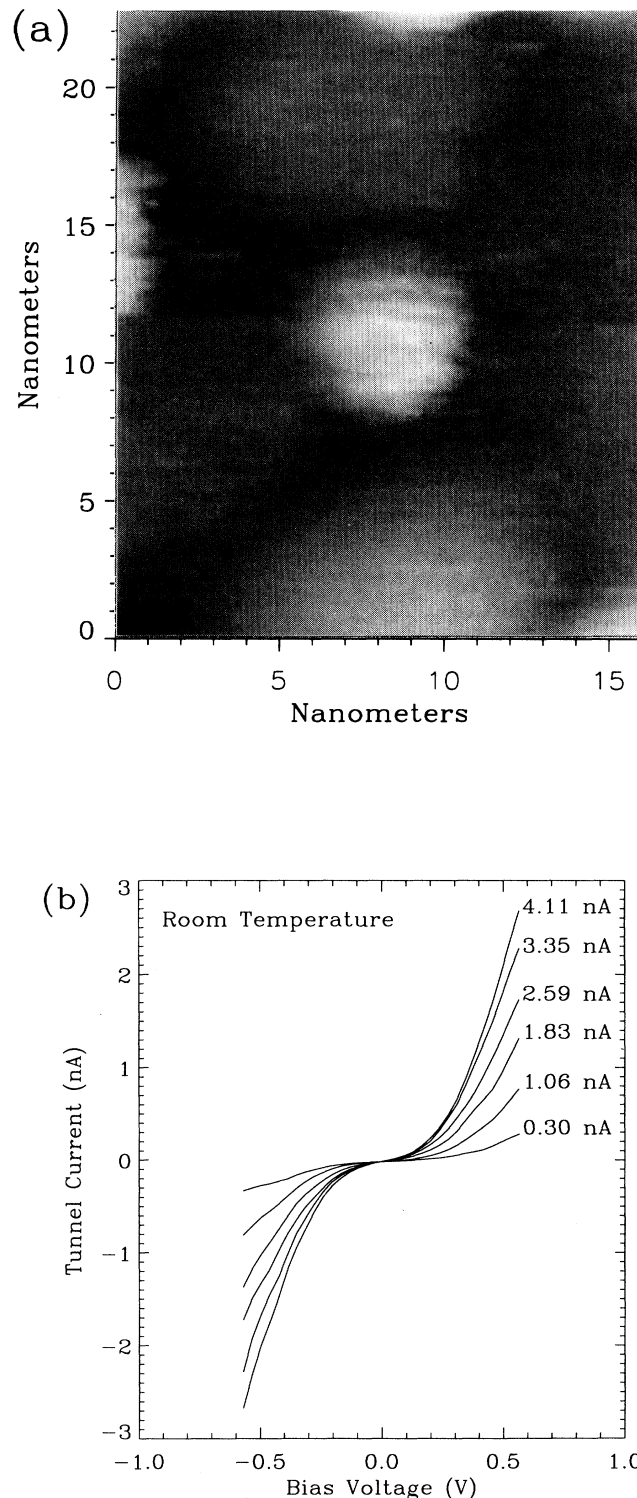


FIG. 2. (a) $16 \text{ nm} \times 23 \text{ nm}$ STM image of a 1.2 nm Au cluster on a XYL dithiol/Au(111) substrate. A tunnel current of 0.6 nA and a bias voltage of -750 mV were used to obtain this image. (b) Corresponding $I(V, z)$ data taken simultaneously in the center of the image shown in (a). The tunnel current set point used to fix the tip-cluster separation is listed beside each curve. The bias voltage set point was -750 mV .

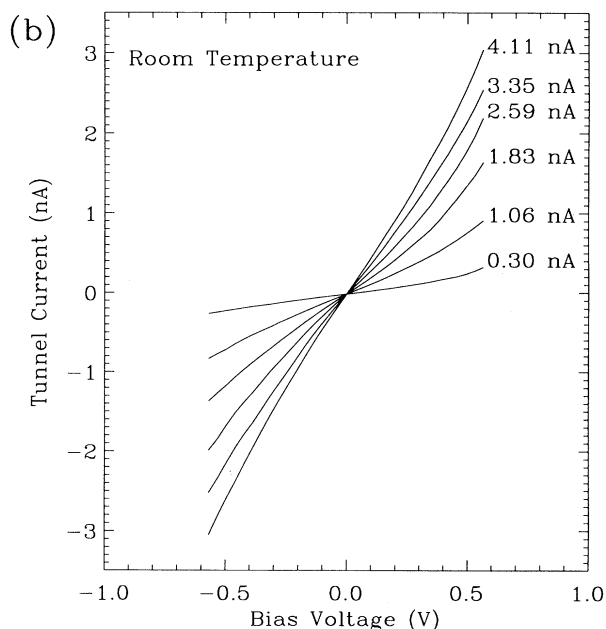
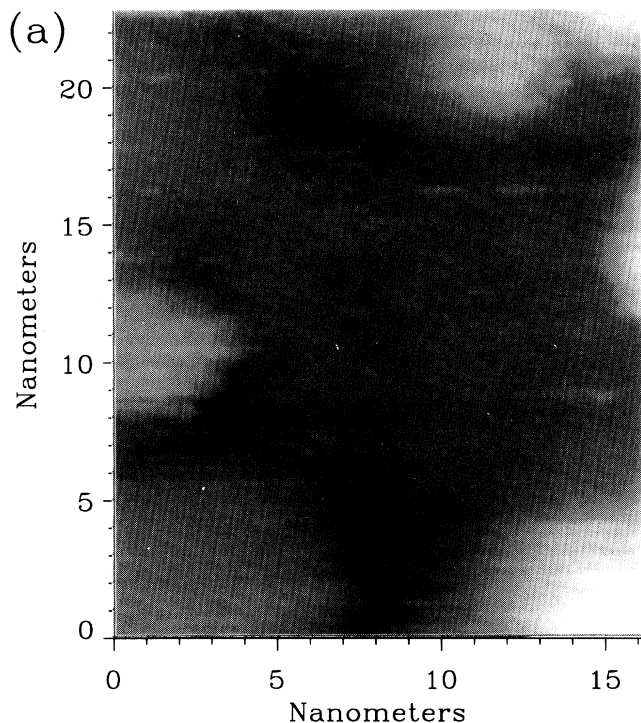


FIG. 3. (a) $16 \times 23 \text{ nm}^2$ STM image centered over the XYL dithiol SAM. A tunnel current of 0.6 nA and a bias voltage of -750 mV were used to obtain this image. (b) Corresponding $I(V, z)$ data taken simultaneously in the center of the image shown in (a). The tunnel current set point used to fix the tip-substrate separation is listed beside each curve. The bias voltage set point was -750 mV .

is impractical since numerical calculations of the partial derivatives are too unwieldy. Alternatively, a search over a wide range of parameters at a coarse resolution and then narrowing in on the best prospects can lead to a local rather than global best fit. Our approach was to use the gap around $V = 0$, and the overall slope of the $I(V)$ curve to put limits on the range of values over which our variables could change and then to perform a thorough search for a best fit within this realistic range. This procedure has been used successfully by us before as reported elsewhere.^{27,28}

Fits to the data in Fig. 2(b) are plotted in Fig. 4 as a function of the set-point tunnel current. These fits are useful to determine if the fitting parameters R_1 , C_1 , R_2 , and C_2 behave reasonably as the tip-cluster separation varies. The rapid decrease in the tunnel resistance R_2 as the tip-cluster separation decreases is recovered from the fitting procedure. The capacitance $C_2 \approx 1.5 \times 10^{-20} \text{ F}$ is a factor of 2 smaller than the expected capacitance in vacuum between a tip of radius $\sim 10 \text{ nm}$ (estimated from the STM image) separated by 0.5 nm from a 1.2 nm diameter cluster. The resistance R_1 and capacitance C_1 between the cluster-substrate remains stationary as the tip separation changes.

It is useful to compare the values R_1 and C_1 to expectations based on the well characterized nature of the nanostructure under study. If the cluster is modeled as

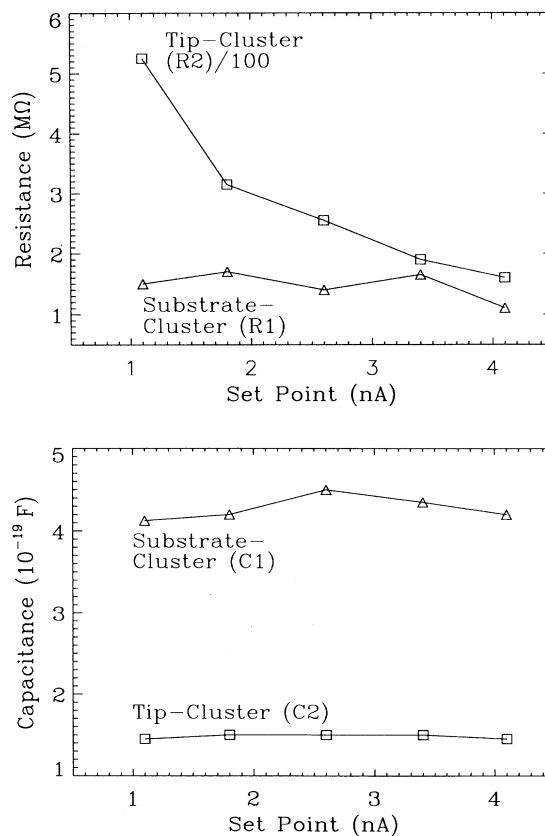


FIG. 4. Plot of fitting parameters as a function of the set point tunneling current for the $I(V, z)$ data shown in Fig. 2.

a sphere, then a classical calculation of its capacitance can be performed.²⁹ For instance, a 1.2 nm diam sphere (i.e., the cluster height measured by STM) suspended in vacuum above a conducting plane by 1 nm (i.e., the estimated thickness of the XYL dithiol layer, 0.83 nm, plus the estimated length of a Au-S bond, ~ 0.2 nm) yields a capacitance of $C_1 \simeq 8.2 \times 10^{-20}$ F. This result is about a factor of 5 smaller than the value of C_1 found in Fig. 4. Including the measured dielectric constant of the XYL dithiol layer from ellipsometry²² (~ 1.5) goes some way toward explaining this discrepancy and suggests that an even higher dielectric constant may be appropriate. Other considerations, like the faceted nature of the cluster and contributions to the capacitance due to fringing fields, may be required before the fitted value of C_1 is quantitatively understood.

IV. ESTIMATING THE ELECTRICAL RESISTANCE OF A MOLECULE

From previous studies, it is known that annealed clusters produced by the MECS are fcc single crystals. The lowest-energy shape of these Au clusters is that of a truncated octahedron. When deposited on an atomically flat substrate, these clusters tend to orient with the hexagonal [111] facet normal to the substrate.³⁰ Assuming this to be the case in the present study, it is possible to use the fitting parameters determined above to estimate the electrical resistance of a single XYL dithiol molecule. Such an analysis may provide a better way to characterize the electrical properties of long-chain molecules than sandwiching a monolayer between two macroscopic conducting electrodes. Experiments using macroscopic contacts are often difficult to interpret because current flow through pin-hole imperfections adds unknown contributions to the measured conductivity.

A relation between the area of the hexagonal [111] facet and cluster height can be obtained by considering the geometry of a perfect truncated octahedron [see Fig. 5(a)]. For the case of Au clusters containing 38, 201, 586, 1289, etc. atoms, the area of the (111) facet can be analytically related to the distance between two opposite facets as shown by the plotted points in Fig. 5(b). For clusters not described by a perfect truncated octahedron, an approximate hexagonal area can be inferred by interpolation [see dotted line in Fig. 5(b)]. From this plot, a Au cluster ~ 1.2 nm high having a truncated octahedral structure has a (111) face with a surface area of ~ 1.2 nm².

Electron diffraction studies of alkanthiolates on Au(111) show that the symmetry of the sulfur atoms is hexagonal with an area per molecule of 0.214 nm².^{31–33} Assuming the XYL dithiol molecules order in a way similar to the alkanethiolates, it follows that the 1.2 nm high cluster studied here is supported by about 6 XYL dithiol molecules.

From these considerations and the fitted resistance between the cluster and substrate (R_1), it follows that an estimate for the resistance of one XYL dithiol molecule at room temperature is

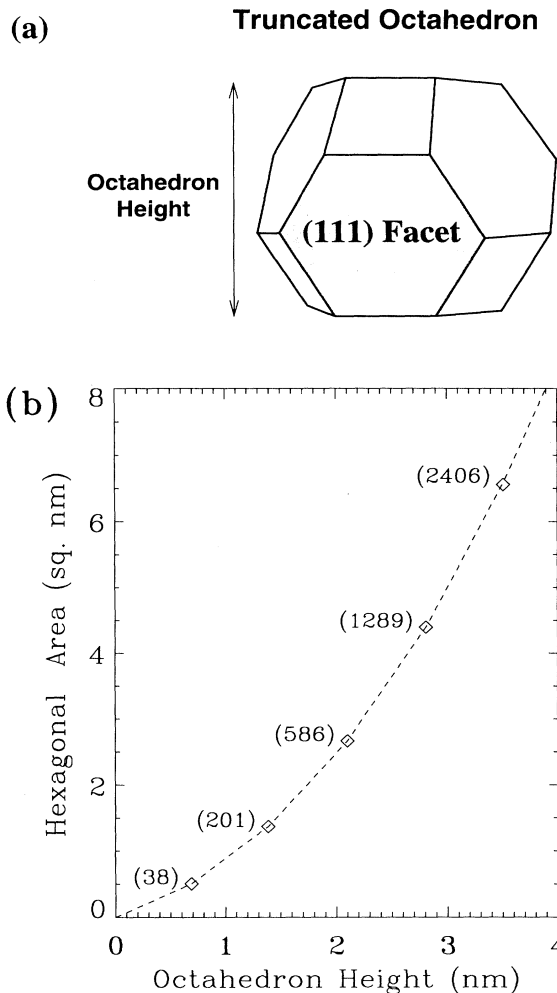


FIG. 5. (a) The geometry of a perfect truncated octahedron. (b) The surface area of a (111) hexagonal facet as a function of octahedron height [the distance between opposite (111) facets]. The number in parentheses next to each plotted point is the number of Au atoms comprising a truncated octahedral cluster of the specified dimensions.

$$R_{\text{molecule}} \simeq 6R_1 \sim 9 \text{ M}\Omega. \quad (1)$$

Not every cluster supported on the XYL dithiol film showed evidence of single-electron effects. This can be explained by a nonuniform coupling of clusters to the substrate, possibly due to irregularities in the XYL dithiol film. This explanation is supported by calculations which show that at room temperature the current suppression at small bias voltage disappears if the capacitance C_1 increases by about a factor of 3. A decrease in the separation between a cluster and the Au film substrate would tend to produce such an increase in C_1 .

To better understand the advantages of a *double-ended* thiol molecule as a cluster support, a separate study was

conducted in which clusters were deposited onto a SAM of a *single-ended* thiol, octadecylthiol. Scanning tunneling microscopy studies of this system indicated that cluster position was often altered by the tip-cluster interaction. Those clusters that were successfully imaged had an average height about 1/2 of that found when similar clusters are supported on a XYL dithiol layer, indicating an increased interaction between the cluster and the underlying substrate. This observation is consistent with the ion-scattering studies reported by Herdt and Czanderna, which indicate penetration of Au atoms at room temperature through an alkanethiol film.⁵ In addition, no evidence for suppression of current near zero bias voltage (Coulomb blockade behavior) was observed when the single-ended thiol was used, another result consistent with the hypothesis of increased coupling between cluster and substrate.

V. DISCUSSION AND CONCLUSIONS

Scanning tunneling microscopy experiments to study the electronic coupling of Au clusters separated from a flat Au substrate by a self-assembling monolayer of XYL dithiol have been described. Because double-ended thiol molecules are used as the spacer layer in this experiment, the position of the clusters remained fixed during repeated scans with the STM tip, allowing reliable stud-

ies of the $I(V)$ characteristics of individual supported clusters. Experiment shows that the supported clusters exhibit a reproducible suppression of current near zero bias voltage, indicating that Coulomb blockade effects at room temperature can be achieved with this system. From a fit to $I(V, z)$ data, the electrical resistance of a single XYL dithiol molecule is estimated to be about 9 M Ω .

Based on these results, systematic studies of the electrical properties of preformed clusters supported on other self-assembled monolayers of dithiols seem particularly interesting. The ability to achieve a controllable geometry manifesting room-temperature Coulomb blockade is particularly noteworthy. Furthermore, by utilizing the known minimum energy structure of annealed clusters, estimates for the electrical resistance of a variety of different self-assembling molecules can also be obtained.

ACKNOWLEDGMENTS

The authors would like to thank Professor S. Datta and Professor C. Kubiak for many helpful discussions and are indebted to Dr. T.G. Miller for providing the computer code used to perform a least squares fit to the tunneling conductance data. This work was partially funded by the Army Research Office URI Program under Contract No. DAAL03-G-0144.

- ¹ R.G. Nuzzo and D.L. Allara, *J. Am. Chem. Soc.* **105**, 4481 (1983).
- ² C.D. Bain and G.M. Whitesides, *Angew. Chem. Ed. Engl.* **28**, 506 (1989).
- ³ P.E. Laibinir, R.G. Nuzzo, and G.M. Whitesides, *J. Phys. Chem.* **96**, 5097 (1992).
- ⁴ D. Anselmetti, T. Richmond, A. Baratoff, G. Borer, M. Dreier, M. Bernasconi, and H.J. Guntherodt, *Europhys. Lett.* **25**, 297 (1994).
- ⁵ G.C. Herdt and A.W. Czanderna, *J. Vac. Sci. Technol. A* **12**, 2410 (1994).
- ⁶ J-P. Bucher, L. Santesson, and K. Kern, *Langmuir* **10**, 979 (1994).
- ⁷ A.N. Patil, D.Y. Paithankar, N. Otsuka, and R.P. Andres, *Z. Phys. D* **26**, 135 (1993).
- ⁸ A.M. Baro, A. Bartolome, L. Vazquez, N. Garcia, R. Reifengerger, E. Choi, and R.P. Andres, *Appl. Phys. Lett.* **51**, 1594 (1987).
- ⁹ D.M. Schaefer, A. Ramachandra, R.P. Andres, and R. Reifengerger, *Z. Phys. D* **26**, S249 (1993).
- ¹⁰ Seung Bin Park, Ph.D. thesis, Purdue University, 1988.
- ¹¹ E. Choi and R.P. Andres, in *Physics and Chemistry of Small Clusters*, edited by P. Jena, B.K. Rao, and S.N. Khanna (Plenum Press, New York, 1987), p. 61.
- ¹² T. Castro, Y.Z. Li, R. Reifengerger, E. Choi, S.B. Park, and R.P. Andres, *J. Vac. Sci. Technol. A* **7**, 2845 (1989).
- ¹³ M.E. Lin, R. Reifengerger, and R.P. Andres, *Phys. Rev. B* **46**, 15 490 (1992).
- ¹⁴ M.E. Lin, R. Reifengerger, A. Ramachandra, and R.P. Andres, *Phys. Rev. B* **46**, 15 498 (1992).
- ¹⁵ T. Castro, R. Reifengerger, E. Choi, and R.P. Andres, *Surf. Sci.* **234**, 43 (1990).
- ¹⁶ T. Castro, R. Reifengerger, E. Choi, and R.P. Andres, *Phys. Rev. B* **42**, 8548 (1990).
- ¹⁷ T. Castro, E. Choi, Y.Z. Li, R.P. Andres, and R. Reifengerger, in *Clusters and Cluster-Assembled Materials*, edited by R. S. Averback, J. Bernhole, and D. L. Nelson, MRS Symposia Proceedings Vol. 206 (Materials Research Society, Pittsburgh, 1991), p. 159.
- ¹⁸ M.E. Lin, A. Ramachandra, R.P. Andres, and R. Reifengerger, in *Nanosources and Manipulation of Atoms under High Fields and Temperatures: Applications*, edited by B. Vu Thein, N. Garcia, and K. Dransfeld (Kluwer Academic Publishers, Boston, 1993), pp. 77-88.
- ¹⁹ R. Piner and R. Reifengerger, *Rev. Sci. Instrum.* **60**, 3123 (1989).
- ²⁰ T.G. Miller, M.W. McElfresh, and R. Reifengerger, *Phys. Rev. B* **48**, 7499 (1993).
- ²¹ J.A. Derose, T. Thundat, L.A. Nagahara, and S.M. Lindsay, *Surf. Sci.* **256**, 102 (1991).
- ²² R.G. Osifchin, R.P. Andres, M. Dorogi, S. Feng, J.I. Henderson, T. Bein, and C.P. Kubiak (unpublished).
- ²³ W. Mahoney, D. M. Schaefer, A. Patil, R. P. Andres, and R. Reifengerger, *Surf. Sci.* **316**, 383 (1994).
- ²⁴ I.O. Kulik and R.I. Shekhter, *Zh. Eksp. Teor. Fiz.* **68**, 623 (1975) [*Sov. Phys. JETP* **41**, 308 (1975)].
- ²⁵ M. Amman, R. Wilkins, E. Ben-Jacob, P.D. Maker, and R.C. Jaklevic, *Phys. Rev. B* **43**, 1146 (1991).

- ²⁶ A.E. Hanna and M. Tinkham, *Phys. Rev. B* **44**, 5919 (1991).
- ²⁷ T.G. Miller, R. Reifenberger, M.W. McElfresh, D.W. Face, and W.L. Holstein, *J. Low Temp. Phys.* **94**, 239 (1994).
- ²⁸ T.G. Miller and R. Reifenberger, *Phys. Rev. B* **50**, 3342 (1994).
- ²⁹ P. Lorrain and D. Corson, *Electromagnetic Fields and Waves*, 2nd ed. (W.H. Freeman and Co., San Francisco, 1970).
- ³⁰ W. Mahoney, S.T. Lin, and R.P. Andres (unpublished).
- ³¹ L. Strong and G.M. Whitesides, *Langmuir* **3**, 546 (1988).
- ³² C.E.D. Chidsey and D.N. Loiacono, *Langmuir* **6**, 709 (1990).
- ³³ L.H. Dubois, B.R. Zegarski, and R.G. Nuzzo, *J. Chem. Phys.* **98**, 678 (1993).

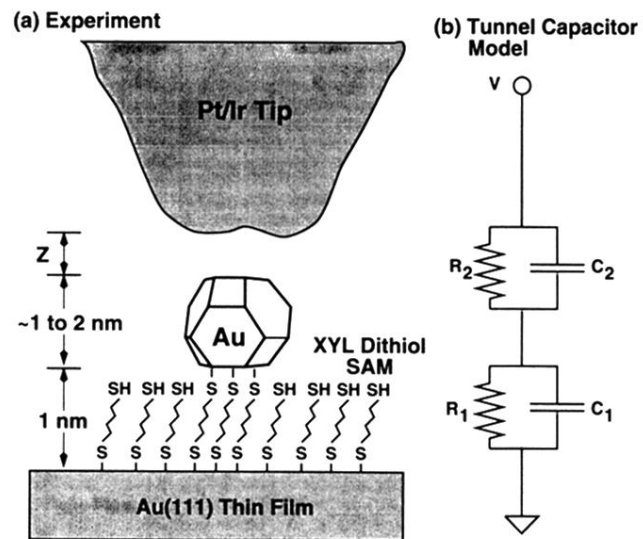


FIG. 1. (a) Schematic diagram of the nanostructure studied. (b) Double junction model used to explain the $I(V)$ data.

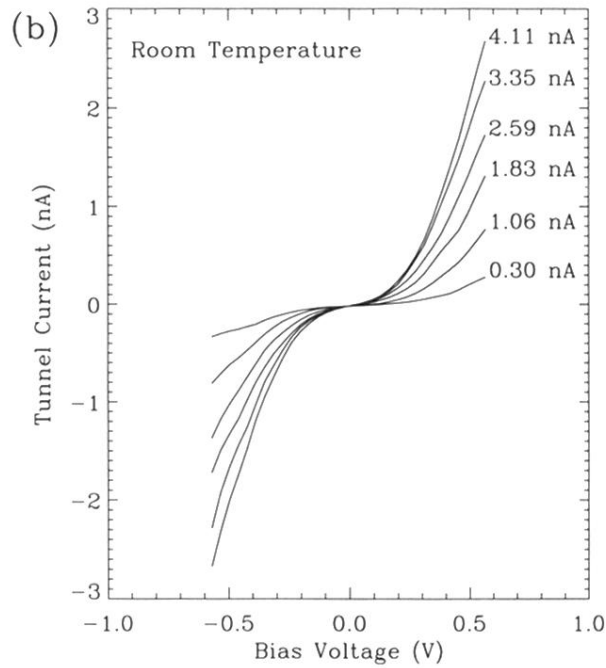
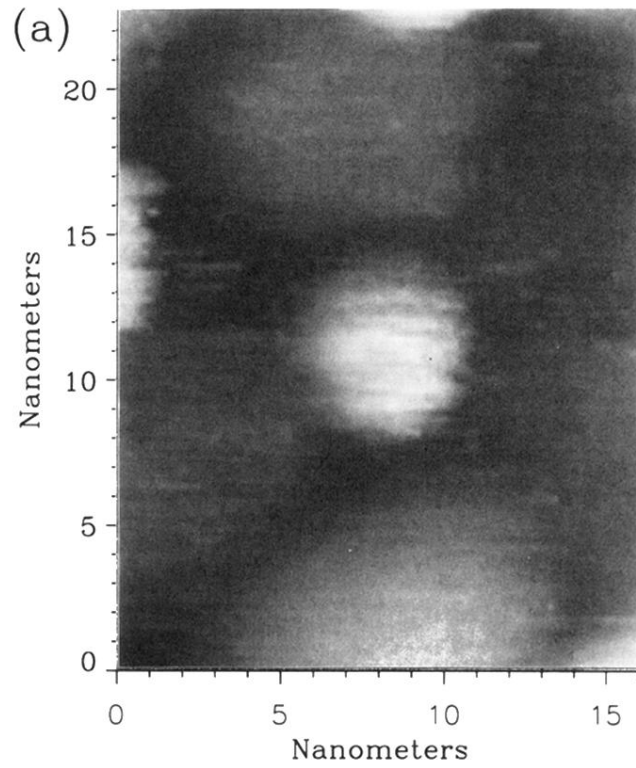


FIG. 2. (a) $16 \text{ nm} \times 23 \text{ nm}$ STM image of a 1.2 nm Au cluster on a XYL dithiol/Au(111) substrate. A tunnel current of 0.6 nA and a bias voltage of -750 mV were used to obtain this image. (b) Corresponding $I(V, z)$ data taken simultaneously in the center of the image shown in (a). The tunnel current set point used to fix the tip-cluster separation is listed beside each curve. The bias voltage set point was -750 mV .

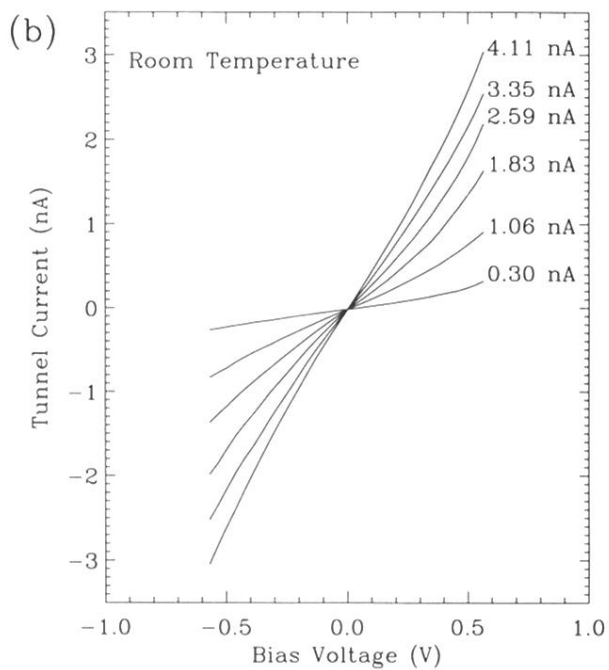
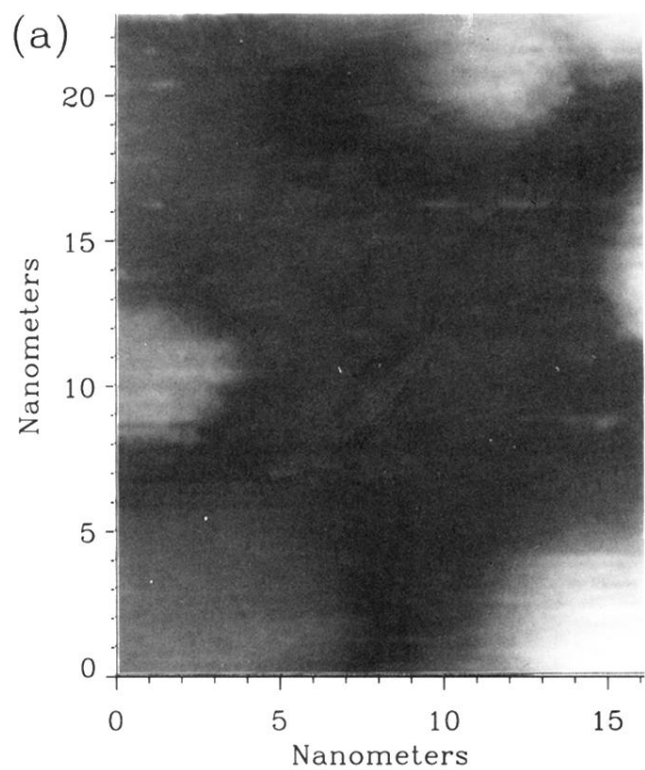


FIG. 3. (a) $16 \times 23 \text{ nm}^2$ STM image centered over the XYL dithiol SAM. A tunnel current of 0.6 nA and a bias voltage of -750 mV were used to obtain this image. (b) Corresponding $I(V, z)$ data taken simultaneously in the center of the image shown in (a). The tunnel current set point used to fix the tip-substrate separation is listed beside each curve. The bias voltage set point was -750 mV .

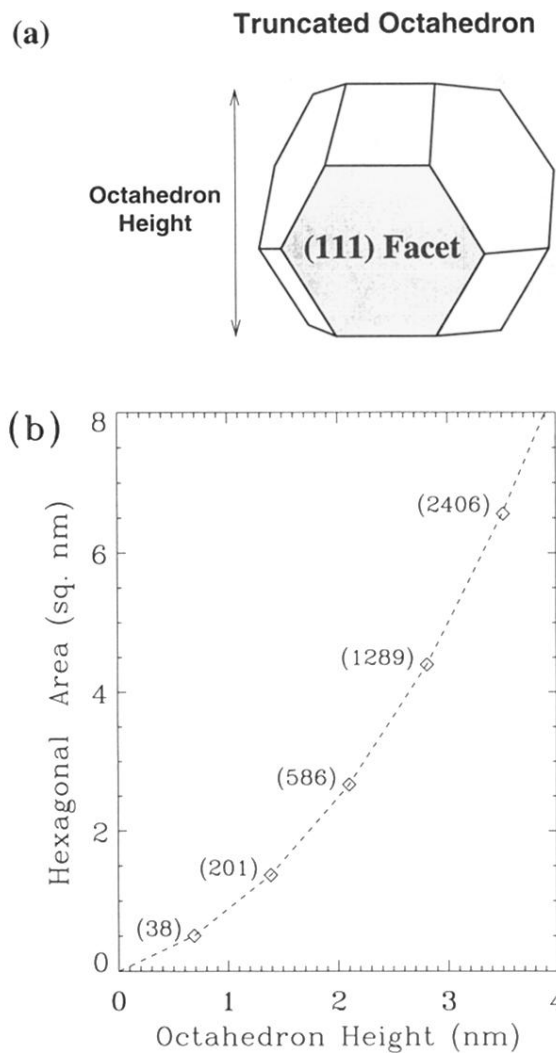


FIG. 5. (a) The geometry of a perfect truncated octahedron. (b) The surface area of a (111) hexagonal facet as a function of octahedron height [the distance between opposite (111) facets]. The number in parentheses next to each plotted point is the number of Au atoms comprising a truncated octahedral cluster of the specified dimensions.